ADVANCED FUNCTIONAL MATERIALS
www.afm-journal.de

www.MaterialsViews.com

Dendrimer-Encapsulated Ruthenium Oxide Nanoparticles as Catalysts in Lithium-Oxygen Batteries

Priyanka Bhattacharya, Eduard N. Nasybulin, Mark H. Engelhard, Libor Kovarik, Mark E. Bowden, Xiaohong S. Li, Daniel J. Gaspar, Wu Xu, and Ji-Guang Zhang**

Dendrimer-encapsulated ruthenium oxide nanoparticles (DEN-RuO_2) have been used as catalysts in lithium-oxygen (Li-O_2) batteries for the first time. The results obtained from ultraviolet-visible spectroscopy, electron microscopy and X-ray photoelectron spectroscopy show that the nanoparticles synthesized by the dendrimer template method are ruthenium oxide, not metallic ruthenium as reported by other groups. The DEN-RuO_2 significantly improves the cycling stability of Li-O_2 batteries with carbon electrodes and decreases the charging potential even at ten times less catalyst loading than those reported previously. The monodispersity, porosity, and large number of surface functionalities of the dendrimer template prevent the aggregation of the RuO_2 nanoparticles, making their entire surface area available for catalysis. The potential of using DEN-RuO_2 as a standalone cathode material for Li-O_2 batteries is also explored.

1. Introduction

A high demand for energy density and safety as well as environmental concerns for transportation and consumer electronics devices has led to the rapid development of energy storage systems that are beyond the state-of-the-art of rechargeable Li-ion batteries. Among these advanced batteries, Li-O_2 batteries are regarded as one of the most promising candidates because of their very high theoretical specific energy (~3500 Wh/kg). In these batteries, O_2 as the active cathode material can be absorbed from the surrounding environment instead of stored in the battery like cathode materials used in Li-ion batteries. However, several critical barriers still need to be overcome before the practical application of Li-O_2 batteries.[1] One of the critical challenges with the Li-O_2 battery is oxidation of the insoluble, poorly conducting Li_2O_2 discharge product during charging.[2] This results in large over-potentials especially during charging and therefore low round-trip efficiency of the battery. Hence, electrocatalysts are required to reduce charging over-potentials and improve the energy efficiency of Li-O_2 batteries.[3,4] In the last few years, significant work has been devoted to the development of efficient electrocatalysts for the oxygen evolution reaction (OER).[2,5] Recent published works indicate that Ru is an effective electrocatalyst for the OER.[6–9] However, a large amount (30–40% of the electrode weight) of Ru has been used in these studies which largely increased their materials cost. Therefore, new approaches that can effectively disperse Ru catalysts and improve the catalytic activity of Ru particles are required for their practical applications.

It is well known that catalytic activity of metal nanoparticles is strongly controlled by the size, stability, solubility, and monodispersity of the particles, and also the chemical and structural nature of the materials from which they are made. Therefore, good synthetic control to achieve these desired parameters is essential for the optimum performance of metal nanoparticles. Poly(amidoamine) (PAMAM) dendrimers are particularly attractive candidates as templates for the synthesis of nanoparticles because they contain a high density of interior tertiary amine groups that can complex with metal ions and variable surface groups to tailor their solubility.[10–17] PAMAM dendrimers are synthetic, highly branched, symmetrical and porous macromolecular architectures that have well-defined interiors.[13] They not only act as templates for the nanoparticles but also stabilize them, thus preventing them from aggregating. Therefore, they have been widely used in the catalysis of hydrogenation of unsaturated organic molecules,[18–20] for oxygen reduction reaction (ORR) and other applications.[21–23] However, the application of DENs as catalysts in advanced energy storage systems such as rechargeable Li-O_2 batteries is still unexplored.

Here, we show that DENs can be used as a template to effectively disperse Ru particles used as the catalyst in Li-O_2 batteries. Contrary to earlier reports by others,[24–27] we demonstrate that Ru encapsulated within the dendrimer exists primarily in its oxidized form, RuO_2, but not in its metallic form, as evidenced by XPS and high-resolution transmission electron microscopy (HRTEM) results. In other words, the Ru nanoparticles formed after reduction from their Ru^{3+} oxidation state

Dr. P. Bhattacharya, Dr. E. N. Nasybulin, X. S. Li, Dr. D. J. Gaspar, Dr. W. Xu, Dr. J.-G. Zhang
Energy and Environment Directorate
Pacific Northwest National Laboratory
Richland, WA 99354, USA
E-mail: priyanka.bhattacharya@pnnl.gov; jiguang.zhang@pnnl.gov
M. H. Engelhard, Dr. L. Kovarik, Dr. M. E. Bowden
Environmental and Molecular Sciences Laboratory
Pacific Northwest National Laboratory
Richland, WA 99354, USA

DOI: 10.1002/adfm.201402701

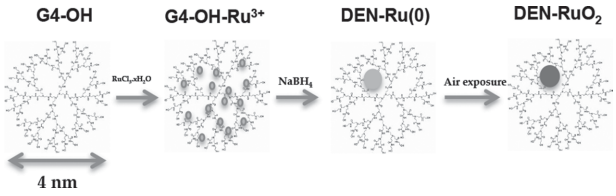

Scheme 1. Schematic of the formation of DEN-RuO_2. G4-OH complexes with Ru^{3+} (small gray circles) from $RuCl_3.xH_2O$ precursor. The complex is reduced chemically using $NaBH_4$ to form DEN-Ru(0) (light gray circle), which readily gets oxidized to DEN-RuO_2 (dark gray circle) on exposure to air.

are quickly oxidized to RuO_2 post-synthesis after exposure to O_2. The feasibility of using DENs to replace traditional carbon-based functional electrode materials in Li-O_2 batteries is also investigated.

2. Results and Discussion

2.1. Preparation and Characterization of DEN-Ru

Scheme 1 shows the synthesis of DEN-Ru using G4-OH dendrimers with 62 interior tertiary amine groups. Three different G4-OH:Ru^{3+} stoichiometric ratios at 1:20, 1:40, and 1:60 were used to synthesize the DEN-Ru. It was found that the catalytic effect towards OER was similar for all the three ratios, so DEN-Ru with G4-OH:Ru^{3+} ratio of 1:20 was chosen to discuss the best cycling performance of the Li-O_2 batteries as below. The entire synthesis was carried out in inert atmosphere (i.e., under nitrogen, N_2) to prevent oxidation of Ru as reported earlier.[24–27] The details of the synthesis procedure can be found in the experimental section of this work.

Figure S1A (in the Supporting Information) shows the characteristic ultraviolet-visible (UV–Vis) absorbance peaks of the G4-OH dendrimers, $RuCl_3.xH_2O$, G4-Ru^{3+} complex, and the DEN-Ru nanoparticles. The size-distribution of the well-dispersed, spherical nanoparticles is narrow, ranging from 1.6 to 2.8 nm with an average size of 2.1 nm (Figure S1B in the Supporting Information). Observations of the relatively well-ordered nanoparticles at the atomic scale show that the Ru nanoparticles have both metallic and oxide characteristics (**Figure 1**A–C). In general, we observed that the smaller particles (<2 nm) tend to have a metallic hexagonal closed packed structure as shown in Figure 1A. In this example, the metallic particle of Ru is oriented along the [211] direction. The corresponding Fast Fourier Transformation (FFT) showing the characteristic d-spacing (2.03 and 2.04 Å indicative of Ru_{011} and Ru_{111} planes, respectively)[28] and inter-planer angles are shown in Figure 1B. This result confirms the metallic character of this nanoparticle. The corresponding simulation of the diffraction pattern is shown in Figure 1C. On the other hand, the larger nanoparticles (>2 nm) display the characteristic d-spacing (d_{110} = 3.14 Å), which is consistent with RuO_2.[29] In many of these observations, the larger particles appear as a result of agglomeration during TEM sample preparation. The presence of oxide nanoparticles suggests that the as-prepared nanoparticles from reduction reaction can be rapidly oxidized during exposure to atmospheric conditions and in aqueous solutions. Interestingly, however, metallic nanoparticles are also observed. While it is possible that a subset of the nanoparticles stay in the reduced state, it is more likely that these nanoparticles were reduced during the electron beam exposure. It is well known that the electron beam has a strong reducing effect, and at the nanoscale, reduction can occur rapidly.[30]

In addition, high-angle annular dark field scanning TEM (HAADF-STEM) imaging was used to analyze the enhanced z-contrast for Ru for the possible presence of sub-nanometer-size clusters. Indeed, the HAADF-STEM analysis (Figure S2 in the Supporting Information) showed the presence of <1 nm

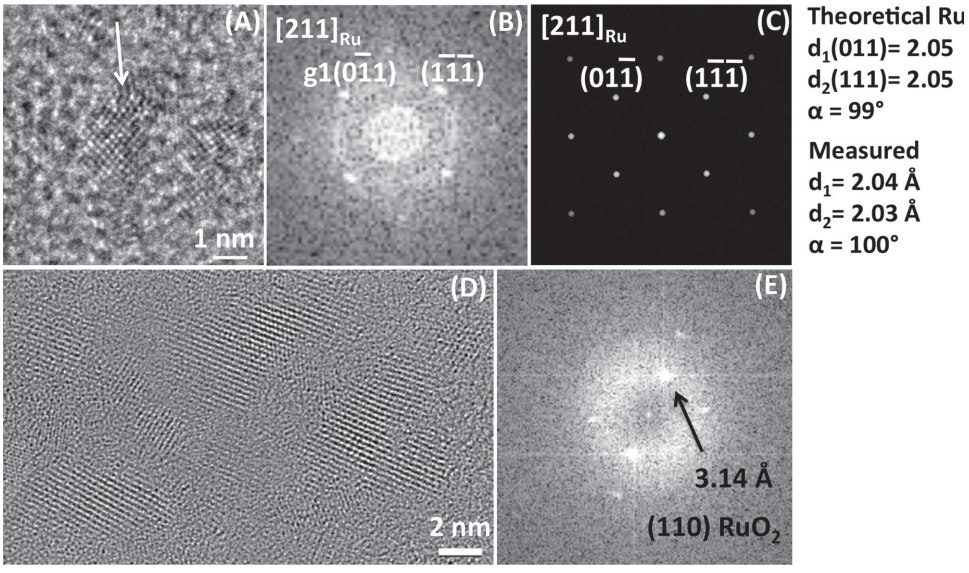

Figure 1. A) HRTEM image of DEN-Ru drop-casted and dried on a carbon-coated copper grid. B) FFT of (A). Lattice spacings indicate presence of metallic Ru (d_{011} = *2.04Å and* d_{111} = *2.03Å* planes). C) Theoretical diffraction pattern of metallic Ru. D) STEM image of DEN-Ru drop-casted and dried on an ultrathin carbon-coated copper grid. E) FFT of (D) showing lattice spacings indicative of RuO_2 (d_{110} = *3.14Å* planes).

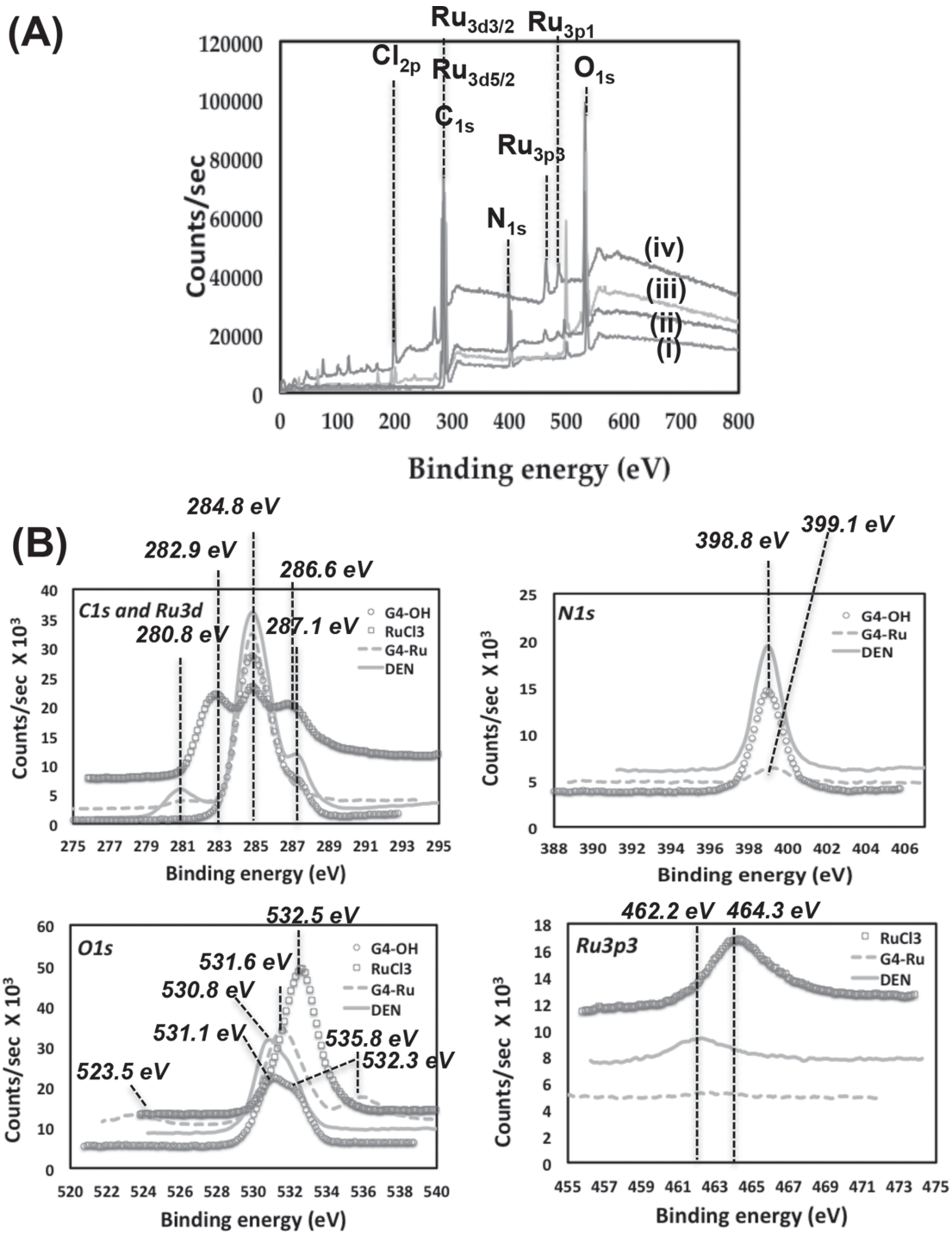

Figure 2. A) XPS survey scan of i) G4-OH, ii) DEN-RuO_2, iii) G4-OH-Ru^{3+} complex, and iv) $RuCl_3{\cdot}xH_2O$ precursor. B) High-energy XPS spectra of C, N, O, and Ru regions of the precursors and the DEN-RuO_2.

clusters of particles, suggesting the co-existence of sub-nanometer clusters of Ru atoms along with the nanoparticle encapsulated within the dendrimer. Their plausible contribution to catalysis and the catalytic activities of these sub-nanometer clusters are yet to be explored.

X-ray photoelectron spectroscopy (XPS) was used to corroborate the TEM observation of the presence of RuO_2 nanoparticles. **Figure 2**A shows the survey scan of the precursors and the DEN-Ru coated on a silicon wafer. The only species observed were C, N, O, and Ru. These results confirm the absence of impurities such as Cl, B, and Na associated with the DEN-Ru synthesis and post dialysis. Figure 2B shows the results from the high-energy resolution XPS analysis of the C, N, O, and Ru regions. Ru_{3d} and Ru_{3p} peaks in the spectra of $RuCl_3{\cdot}xH_2O$ were

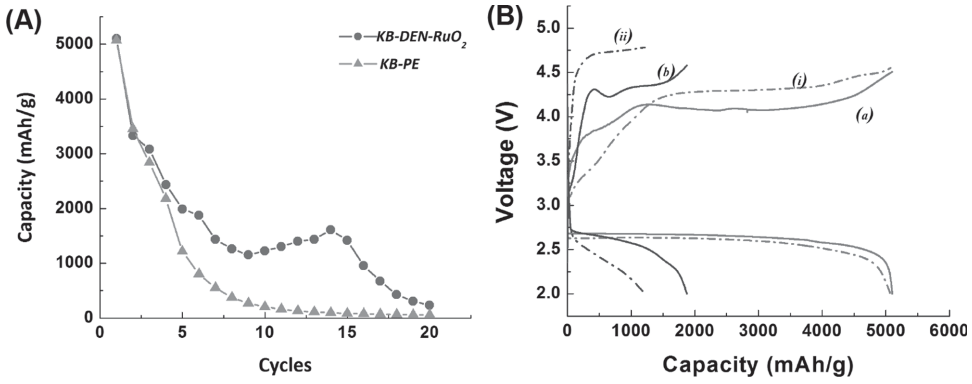

Figure 3. A) Capacity-voltage profile of Li-O_2 coin cells with KB-PE only (triangular markers) and KB-DEN-RuO_2 (circular markers) composite cathodes. B) Voltage profiles of the first and fifth cycles of batteries with KB-PE only electrodes (*(i),(ii)*) and KB-DEN-RuO_2 electrodes (*(a),(b)*) as discussed in section 2.2.

referenced to the position of the most intense carbon peak at 284.8 eV associated with the C1s level of hydrocarbon contaminants.[31] Note that both 3p and 3d photoelectrons are observed for Ru; because Ru overlaps with many other elements (especially carbon) the 3p region is the most commonly studied.[32] The $RuCl_3{\cdot}xH_2O$ precursor has a $Ru_{3d5/2}$ peak at 282.9 eV and a $Ru_{3d3/2}$ peak at 286.6 eV.[31] The $Ru_{3p3/2}$ peak at 464.3 eV, however, suggests that the starting material contains higher oxidation species, such as chlorohydroxo species of Ru^{4+}.[33] The O1s spectrum shows the oxygen peak associated with water molecules at 532.5 eV.[34] In the spectra of the uncomplexed dendrimer, a peak at 287.1 eV is observed and assigned to the group of C-OH, C-N(amine), and C-N(amide) carbons.[35] The O1s spectrum consists of two peaks at 531.1 eV and 532.3 eV, which correspond to carbonyl and hydroxyl oxygens, respectively, and amine nitrogen peaks are observed at 398.8 eV.[35]

Upon complexation with G4-OH, the $Ru_{3d5/2}$ peak shifts to lower binding energy (280.8 eV), which is consistent with an LMCT interaction between Ru^{3+} and the dendrimer, as seen in the G4-OH-Ru^{3+} complex spectra. The ligand exchange with Cl, which is more electronegative than tertiary amines, results in an increase in the amount of charge localized on the metal ion, and hence, a lowering of its binding energy. The N1s peak on the other hand shifts to a slightly higher binding energy at 399.1 eV. The DEN-Ru spectra shows the $Ru_{3d5/2}$ at 280.8 eV and the $Ru_{3p3/2}$ at 462.2 eV, clearly indicating the presence of RuO_2.[34] The O1s peak at 530.8 eV is indicative of the O within the chemisorbed water in RuO_2.[36] The N1s peak shifts back to 398.9 eV as evidence of de-complexation of Ru^{3+} with the tertiary amines. Table S1 in the Supporting Information shows the binding energies of the XPS peaks. These results indicate that, in aqueous solutions and after even momentary exposure to O_2 at room temperature, metallic Ru nanoparticles undergo oxidation. This indicates the reaction rate between gaseous O_2 and nano-sized metallic Ru particles (<2.5 nm) is indeed high, which is in agreement with previously observed O_2 uptake by Ru crystals.[37–39] These results clearly suggest that RuO_2, not metallic Ru,[24–27] is obtained when the DEN-Ru was synthesized by the conventional dendrimer route in a N_2 atmosphere in aqueous solutions. In this work, therefore, DEN-RuO_2 will be used to represent the functional RuO_2 catalyst encapsulated in a dendrimer.

2.2. Application of DEN-RuO_2 as Catalysts in Li-O_2 Batteries

To test the efficiency of DEN-RuO_2 as the OER catalyst in Li-O_2 batteries, Ketjenblack carbon (KB), which is a commonly used high-surface-area carbon, was chosen as the matrix to store discharge products. In this electrode, DEN-RuO_2 also acted as the binder so no other polymer binder was used. The catalyst was mixed with KB at 4 wt%, which is ten times lower than that used in other studies.[6–8] The loading of each electrode was ~1 mg/cm^2. Considering the high cost of Ru, the method used in this work could thus offer a significant cost-reduction in a catalyzed Li-O_2 electrode compared to previous studies.

The KB-DEN-RuO_2 composites delivered better cycling performance than KB-polyethylene (PE) binder alone (**Figure 3**A). The DEN-RuO_2 composites also were able to reduce the oxidation potential of Li_2O_2 on KB carbon by 0.2 V in the first cycle (Figure 3B *(a)* and *(i)*) and by 0.5 V in subsequent cycles (Figure 3B *(b)* and *(ii)*), which is better than or comparable to the recently reported results mentioned above,[6–8] even using <10 times of the catalyst used in the prior studies. For example, Yilmaz et al. showed a reduction of the OER potential by 0.4V compared with pristine carbon nanotubes by employing RuO_2 catalysts, and 20 charge–discharge cycles with capacity limited to 1000 mAh/g.[8] However, the catalyst loading in their work was very high (32%). In contrast, the KB-DEN-RuO_2 composites in the present work maintain stable cycling up to about 16 cycles, with an average capacity of 1550 mAh/g (1.29 mAh/cm^2) (based on the total weight of the composite), and most of the charging takes place between 4 and 4.4 V, using only 4wt% catalyst. Furthermore, unlike most reported results with depth of discharge limited by capacity, the present samples were fully discharged until voltage dropped to 2 V, and charging was performed until full capacity was recovered. This allowed us to gauge the effect of the catalyst on the maximum discharge capacity of KB carbon as well as to assess the effect of KB-DEN-RuO_2 on electrolyte degradation and vice versa.

The discharge capacity results indicate that there is a significant drop in capacity (~74% for KB-PE and 60% for KB-DEN-RuO_2 composites) between the first and fifth cycles. This initial capacity drop can be attributed to partial blocking of KB carbon pores by the insoluble and only partially rechargeable side-products of electrolyte decomposition. However, the

KB-DEN-RuO_2 composites display stable cycling after 5 cycles up to about 16 cycles, in contrast to KB-PE electrode, whose capacity continues to fade. The charging potential for the KB-PE electrode continues to increase to >4.75 V by the fifth cycle. The increase is due to the formation of insoluble side-products during discharge that are not readily decomposed during charging.[1] In contrast, the KB-DEN-RuO_2 composites are able to maintain a relatively low charging potential of 4.4 V up to the sixteenth cycle. One of the major challenges facing the practical realization of Li-O_2 batteries is side reactions associated with solvent degradation. Much effort is being put into developing stable electrolytes for enhancing battery life with full cycling and low charging overpotentials. Thus the delayed, but still observed, capacity fading in the batteries with KB-DEN-RuO_2 composites is a result of side-reactions between Li_2O_2 and the electrolyte and KB carbon, resulting in blocking of active sites on KB by insoluble side-products (Figure S6F in Supporting Information). Nevertheless, this work demonstrates the potential of using DEN-RuO_2 as catalysts in Li-O_2 batteries. The monodispersity and high available surface area of DEN-RuO_2 for effective catalysis could prove to be advantageous over the conventional, large amount of noble metal catalysts used today. An interesting observation was that the total discharge capacity of the KB-DEN-RuO_2 electrode exceeds that expected from the KB content of the electrode. In other words, about 13% more capacity is achieved based on the KB weight in the electrodes, suggesting that the DEN-RuO_2 provided this added capacity (Figure S3 in Supporting Information). We will discuss this observation in greater detail in section 2.3.

It should be indicated that the electrodes with the KB-DEN-RuO_2 composites also were binder free. The dendrimers are amphiphilic molecules with relatively hydrophobic interiors. This amphiphilicity allows the dendrimers to bind strongly with the hydrophobic KB carbon and disperse them well in aqueous solutions. This strong binding initially shrinks the carbon surface considerably; the carbon surface later expands greatly as electrolyte penetrates during battery cycling. The measured Brunauer-Emmett-Teller (BET) surface area of pure KB carbon is 1547 m^2/g while it is 617.2 m^2/g for the KB-DEN-RuO_2 composites. The pore volume measured by the Barrett-Joyner-Halenda (BJH) method also is significantly reduced, i.e., 4.3 cc/g for KB carbon vs 1.93 cc/g for KB-DEN-RuO_2 composites. Wetting of the dendrimers in polar aprotic solvents, such as tetraglyme as used in this study, is poor, and typically takes a day to achieve complete wetting. Thus, the batteries remained in the glove box for a day after assembly and before testing. Binder-free electrodes can increase the capacity per electrode weight and avoid side reactions of Li_2O_2 discharge products with the binder.[40,41]

2.3. DEN-RuO_2 as Functional Electrodes

To verify the hypothesis that the DEN-RuO_2 electrodes themselves provide some capacity, the DEN-RuO_2 was dispersed in methanol, deposited on a hydrophobic carbon paper substrate and tested its performance in Li-O_2 coin-cell batteries. Indeed, the DEN-RuO_2 showed a capacity of ~0.14 mAh/cm^2 (**Figure 4**A). The capacity measured during the first cycle was only 0.05 mAh/cm^2, which then increased during the second cycle. One explanation for the low capacity during the first cycle may be the poor wetting of the DEN-RuO_2 electrodes by the polar aprotic solvents, which leads to slow penetration of the electrolyte. The low capacity could also be due to the lower surface area of the dendrimers when deposited on carbon paper, and/or the small amount of RuO_2, which does not substantially improve the electronic conductivity of the insulating dendrimers. Nevertheless, the cyclic voltammetry (CV) studies (Figure 4B) showed that these DEN-RuO_2 electrodes are stable with respect to the electrolyte (inset shows CV results in argon (Ar)). They also have a catalytic effect in reducing the OER potential, as seen by the negative shift in the OER potential peak of DEN-RuO_2 deposited on glassy carbon (GC) as compared to the control GC electrode. In comparison to the performance in coin-cell batteries, the voltage measured by CV is lowered by only 76 mV because Li_2O_2 is oxidized at a potential very close to its thermodynamic potential on GC itself. The stability of the DEN-RuO_2 was further evidenced by Raman spectroscopy measurements on

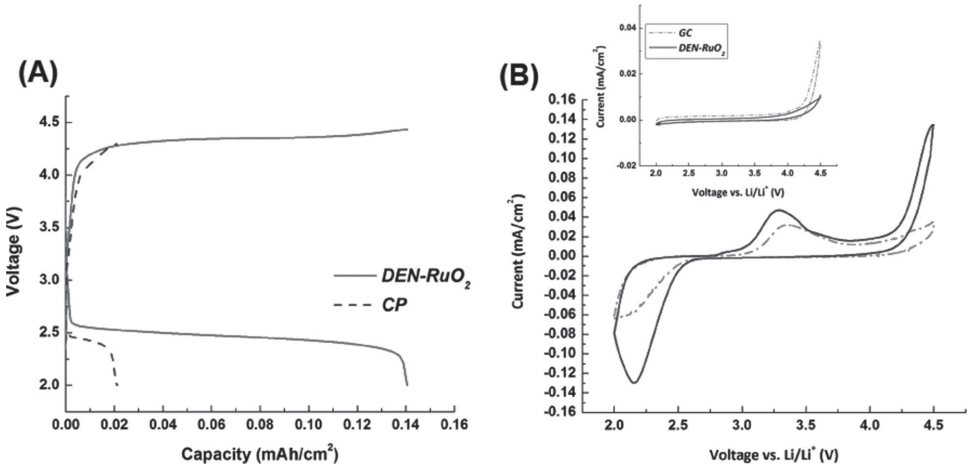

Figure 4. A) Voltage profiles of batteries with DEN-RuO_2 deposited on carbon paper (CP) (solid curve) and control CP as electrodes (dotted curve). B) CV profiles of DEN-RuO_2 electrodeposited on GC electrode (solid curve) and the control GC electrode (dotted curve) in O_2-saturated 1 M LiTf-Tetraglyme and in Ar-saturated 1 M LiTf-Tetraglyme (inset). The scan rate was 20 mV/s.

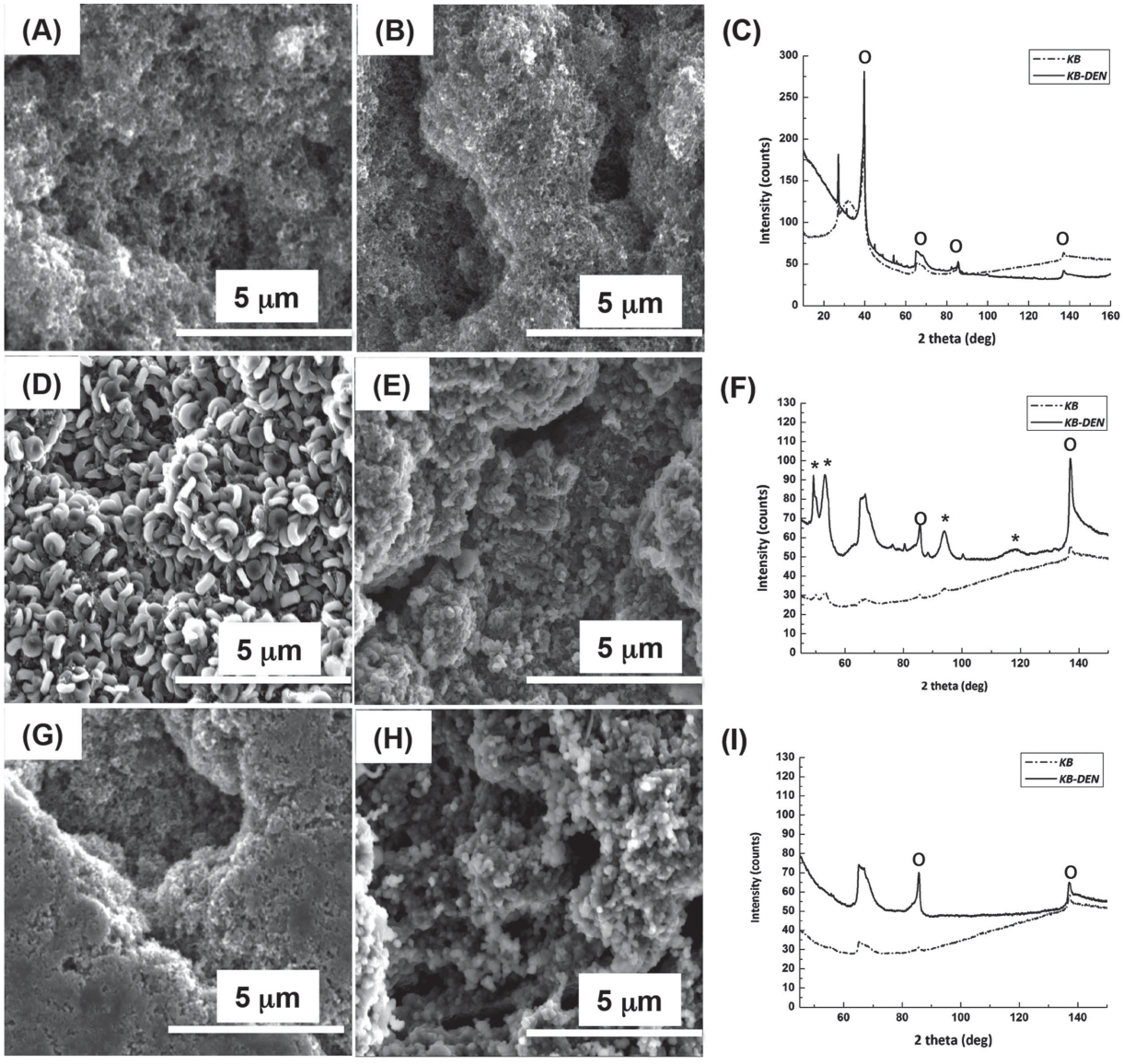

Figure 5. SEM images of pristine A) KB-PE and B) KB-DEN-RuO_2 electrodes and C) their corresponding XRD spectra; first discharge of D) KB-PE and E) KB-DEN-RuO_2 electrodes and F) their corresponding XRD spectra; fifth discharge of G) KB-PE and H) KB-DEN-RuO_2 electrodes and I) their corresponding XRD spectra. Circles (°) in the XRD spectra indicate graphitic carbon peaks while stars (*) indicate crystalline Li_2O_2 peaks.

pristine and charged electrodes after five cycles. The Raman shifts were nearly identical to those previously reported in literature,[42] and correspond to the amide bonds (1500 –1700 cm^{-1}) and –CH bonds (1300 – 1500 cm^{-1}) in the dendrimers. No significant chemical shift was observed between the above electrodes, further implying their electrochemical stability in Li-O_2 cells with tetraglyme-based electrolytes (Figure S4 in the Supporting Information). Based on these results, it is shown that DENs are potentially stable candidates as non-carbon electrodes for Li-O_2 batteries.

2.4. Analysis of Discharge Products

Figure 5 shows scanning electron micrographs (SEM) and X-ray diffraction (XRD) spectra of pristine and discharged (after first and fifth cycle) KB-PE and KB-DEN-RuO_2 electrodes. Figures 5A and 5B show SEM images of pristine KB-PE and KB-DEN-RuO_2 electrodes, respectively. Their corresponding XRD spectra are shown in Figure 5C. No Ru XRD peaks were observed in the KB-DEN-RuO_2 electrodes because of their extremely small size (~2 nm) and the small amount present. The SEM images also appear to confirm the earlier statement that the DEN-RuO_2 shrinks the KB carbon as can be seen in Figure 5B. This shrinking reduces the surface area of the carbon and makes it more difficult for the smaller sized Li_2O_2 structures to be observed.

In Figure 5D, SEM images of the KB-PE electrode after the first discharge, toroid-like shaped Li_2O_2 particles can be clearly seen. In contrast to the KB-PE electrodes, much smaller Li_2O_2 structures are observed in Figure 5E during the first discharge on KB-DEN-RuO_2 composite electrodes. The particles on the

KB-PE electrode are bigger (~500 nm average size) than those on the KB-DEN-RuO_2 composite electrode (~200 nm average size). The corresponding XRD patterns of these initial particles show the crystalline Li_2O_2 phases and the absence of any other side products (Figure 5F). After five cycles, the discharged KB-PE electrodes no longer show the toroidal structures; consistent with previous reports.[43] Instead, a thick layer of discharge products were formed on the KB-PE electrode which could not be identified by XRD because of their amorphous nature (Figure 5G). However, electron diffraction spectra (EDS; Figure S5D inset in the Supporting Information) show these regions to be rich in both carbon and oxygen, which could indicate the deposition of electrolyte degradation products such as Li_2CO_3 as reported earlier.[2,3] After the fifth discharge, the KB-DEN-RuO_2 composite electrode shows the presence of spherical structures that appear to be amorphous, and could not be verified as Li_2O_2 (Figure 5H). However, EDS analysis (Figure S6D in the Supporting Information) indicates the presence of O with a small amount of C, suggesting that only a small amount of electrolyte decomposition occurred on this electrode. Yilmaz et al. have recently shown the poor crystallinity of Li_2O_2 on cathodes comprised of carbon nanotubes with RuO_2 dispersed on them.[8] Poorly crystalline structures are easier to decompose, which would lower the OER potential. Particles composed of the Li_2O_2 discharge product have been reported to have a characteristic toroidal shape only upon the first deep discharge.[1]

Figure 6 shows SEM images of the charged electrodes. For easy comparison, SEM images of pristine KB-PE, KB-DEN-RuO_2

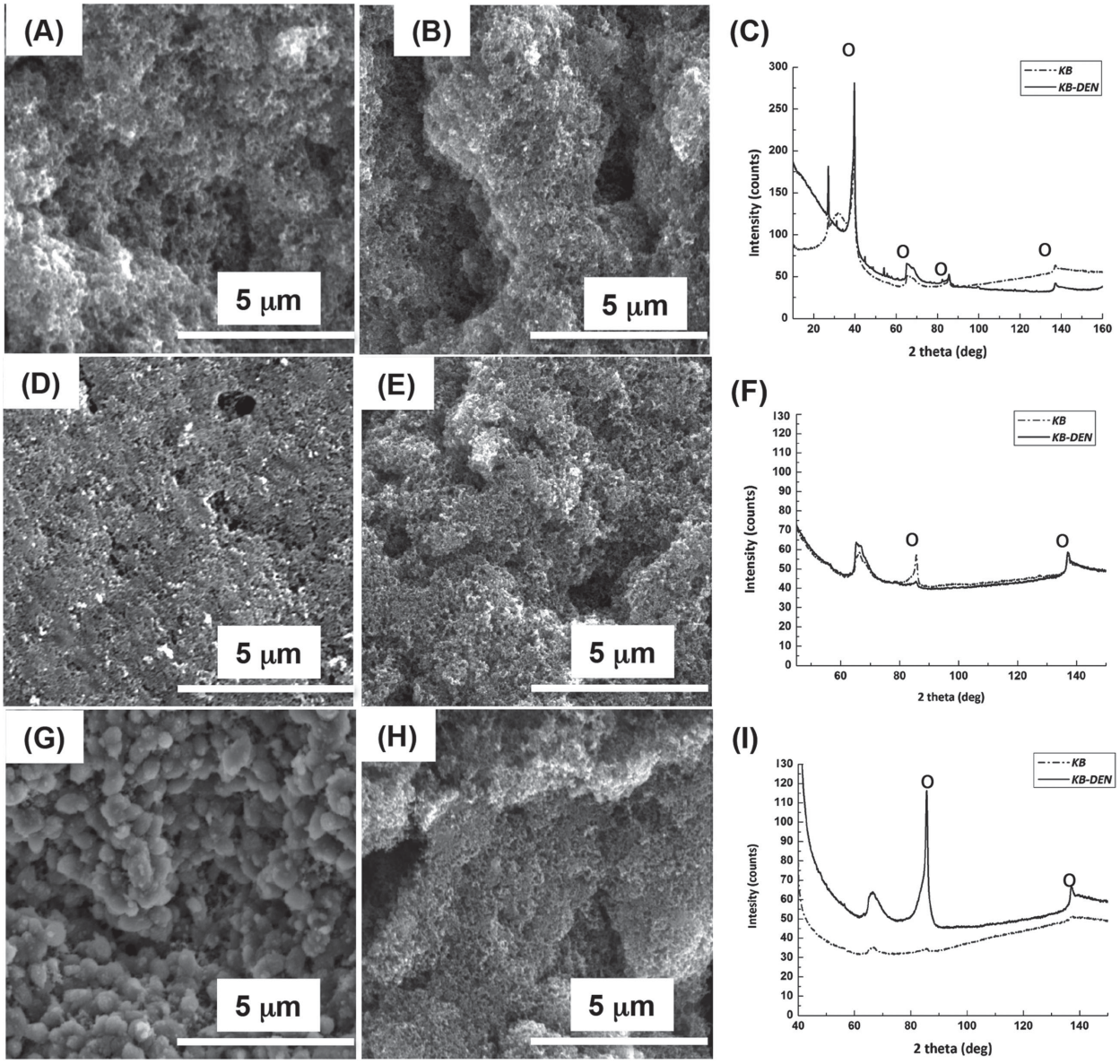

Figure 6. SEM images of pristine A) KB-PE and B) KB-DEN-RuO_2 electrodes and C) their corresponding XRD spectra; first charge of D) KB-PE and E) KB-DEN-RuO_2 electrodes and F) their corresponding XRD spectra; fifth charge of G) KB-PE and H) KB-DEN-RuO_2 electrodes and I) their corresponding XRD spectra. Circles (°) in the XRD spectra indicate graphitic carbon peaks while stars (*) indicate crystalline Li_2O_2 peaks.

electrodes and their corresponding XRD spectra are re-plotted in Figures 6A, 6B, and 6C, respectively. After the first charge, both KB-PE and KB-DEN-RuO_2 electrodes exhibit no Li_2O_2-like structures (Figures 6D and 6E), but their morphologies are similar to those of the pristine samples. However, on the fifth charge, the KB-PE electrode did not completely restore its porosity as shown by the presence of spherical amorphous structures beneath thick, smooth layers (Figure 6G), suggesting incomplete oxidation of the electrolyte decomposition products. Again, because of their amorphous nature, these products could not be identified by XRD. On the contrary, the morphology of KB-DEN-RuO_2 electrodes returned to a pristine state after the fifth charge (Figure 6H and Figure S6E in the Supporting Information). The KB-PE electrode also loses some surface area during the first charge and becomes more compact. As mentioned in section 2.2, the loss of surface area could be the reason behind the capacity fading after the first cycle. It should be pointed out that the XRD peak intensities vary significantly because of the orientations of the graphitic carbon packed in dissimilar ways in different electrodes.

3. Conclusion

Dendrimers have been used in Li-O_2 batteries for the first time as effective scaffolds to disperse RuO_2 catalysts. Ru was chosen to synthesize the DEN-Ru nanocomposites for air electrodes. However, in the aqueous environment, RuO_2 instead of metallic Ru was obtained. STEM and XPS analyses indicated that the monodispersed RuO_2 nanoparticles had a narrow size distribution and an average particle size of 2.1 nm. Also, the reduction of Ru^{3+} precursor ions resulted in the co-formation of sub-nanometer clusters of Ru atoms. Thus, RuO_2 was considered as the active catalyst in catalysis studies involving DEN-RuO_2. When tested in Li-O_2 batteries, DEN-RuO_2 lowered the OER potential by about 0.5 V, at a loading of <10% compared to previous reports, which should significantly reduce the cost of catalyst used in Li-O_2 batteries. In addition, DEN-RuO_2 also improved the cycle life of Li-O_2 batteries. The improved performance could be attributed to the high available surface area coupled with the monodispersity of the DEN-RuO_2. The dendrimer periphery prevented the encapsulated RuO_2 nanoparticles from aggregating, thus making a large fraction of their surface available for catalysis. Although the cycling performance of Li-O_2 batteries with DEN-RuO_2 still needs to be improved, such porous, branched structured DEN-RuO_2 can be regarded as a promising air cathode material for Li-O_2 batteries.

4. Experimental Section

Materials: Generation-four polyamidoamine dendrimers (G4-OH) (10 wt% in methanol, MW = 14,277.19), ruthenium(III) chloride hydrate ($RuCl_3{\cdot}xH_2O$) and sodium borohydride ($NaBH_4$) were purchased from Sigma-Aldrich and used as received. Ketjenblack (KB) carbon (EC-600JD) used for making the air electrodes was purchased from Akzo Nobel Polymer Chemicals. Lithium trifluoromethanesulfonate (LiTf), dimethoxyethane (DME) and tetraethylene glycol dimethyl ether (tetraglyme) solvents were purchased from BASF as battery grades. The tetraglyme was dried over freshly activated 4Å molecular sieves for 1 week before use. Polyethylene (PE) polymer (MW = 34,000) used as binder was purchased from Sigma-Aldrich. Lithium foil discs (99.9%, 1.5 cm in diameter and 1 mm thick) were obtained from MTI corp. These chemicals were stored in an MBraun glovebox filled with purified Ar. Aqueous solutions were prepared using 18 MΩ·cm double-deionized (DI) (NANOpure Diamond Life Science (UV/UF) ultrapure water system) water with total organic carbon <3 ppb and sufficiently purged with N_2 to remove dissolved O_2.

Synthesis of DEN-RuO_2: Prior to use, methanol was evaporated from the G4-OH stock solution under a flow of nitrogen and then G4-OH was re-dissolved in DI water to make a 0.5 mM (8.07 mg/mL) solution. The pH of the G4-OH solution was 8. $RuCl_3{\cdot}xH_2O$ was dissolved in DI water at a concentration of 58.3 mM (12.1 mg/mL). These solutions were used as stocks for the DEN-RuO_2 synthesis. $RuCl_3{\cdot}xH_2O$ was added dropwise to a continuously stirring solution of G4-OH in a N_2 filled glove bag until the molar ratio of G4:Ru^{3+} was 1:20. The solution was stirred for three days to ensure complete complexation between the tertiary amines of G4-OH and Ru^{3+}. The precursor solution was then reduced using 20 molar excess of a freshly prepared aqueous solution of $NaBH_4$ (0.5 M). Caution was taken when slowly adding the $NaBH_4$ solution at a rate of 20 µL/min. The reduction was allowed to proceed to completion in a sealed vial for 24 hours in an N_2 atmosphere. Keeping the reaction vial tightly sealed to ensure the retention of a partial pressure of H_2, a byproduct of the aqueous BH_4^- reduction step, with continuous mixing for a day, completed the reduction process. The reduced DEN-Ru were then dialyzed against DI water using a 10,000 MWCO dialysis membrane (Spectra/Por Float-A-Lyzer, Spectrum Labs) for 24 hours to remove unreacted precursors and impurities. The dialysis was carried out in the N_2 filled glove bag with N_2 purged DI water.

DEN-Based Materials Characterization: UV–VIS spectra were obtained using a Shimadzu UV–Vis–NIR spectrophotometer (model UV-3600) using 1.00 cm quartz cuvettes. All spectra were background-corrected using DI water as a blank. The DEN-Ru, $RuCl_3{\cdot}xH_2O$ and G4-OH solutions were diluted before obtaining the spectra. The final concentrations used are mentioned in Figure S1A. XPS measurements were performed with a Physical Electronics Quantera Scanning X-ray Microprobe. This system uses a focused monochromatic Al Kα X-ray (1486.7 eV) source for excitation and a spherical section analyzer. The instrument has a 32-element multichannel detection system. A 100 W X-ray beam focused to 100 µm diameter was rastered over a 1.2 mm × 0.1 mm rectangle on the sample. The X-ray beam is incident normal to the sample and the photoelectron detector is at 45° off-normal. High-energy resolution spectra were collected using a pass-energy of 69.0 eV with a step size of 0.125 eV. For the $Ag_{3d5/2}$ line, these conditions produced a full width at half maximum (FWHM) of 0.91 eV. A clean silicon wafer was mounted onto a standard Physical Electronics 75 mm × 75 mm sample holder using stainless steel screws. The sample holder is located in a N_2 purged glove box attached to the XPS introduction chamber. The glove box is maintained at <0.2 ppm O_2 with a H_2O dew point of −80 °C. The DEN-RuO_2 nanoparticles were suspended in DI H_2O and pipetted onto the clean silicon wafer and allowed to dry. After the water evaporated, the sample holder was placed into the XPS vacuum introduction system and pumped to $<1 \times 10^{-7}$ Torr using a turbo molecular pumping system prior to introduction into the main ultra-high vacuum system. The main vacuum system pressure is maintained at $<1 \times 10^{-10}$ Torr during analysis and pumped using a series of sputter ion pumps and turbo-molecular pumps. The TEM observations were performed with an aberration corrected FEI Titan 80–300. The imaging was performed both in conventional parallel beam imaging mode and in STEM mode. For the conventional imaging, the images were recorded using a (2k × 2k) charge-coupled device (CCD) camera in Digital Micrograph 1.8. In the STEM mode, the imaging was performed with HAADF detector with a detection angle that is three times higher than the convergence angle. Samples were prepared using both 200-mesh Cu grids coated with Lacey carbon (Figures S1B, 1A-C, S2) and ultrathin carbon film (Figures 1D, E) (Electron Microscopy Sciences). A Cu grid was placed onto a filter paper and a few drops of the DEN-RuO_2 solution

were applied on the grid. Wicking was used to remove any excess sample. Electron diffraction pattern simulations were done using the JEMS software package.

Electrode Preparation, Battery Assembly and Testing: KB-DEN-RuO_2 electrode materials were prepared by mixing an aqueous solution of DEN-RuO_2 with KB carbon at a DEN-RuO_2:KB = 33:67 ratio by weight. The loading of Ru in these samples was 4 wt% (measured by ICP-MS). Mixing continued for one day in a sealed vial. Water then was removed by drying at 80 °C in vacuum overnight. The control KB-PE electrode materials were prepared in a similar way by mixing KB carbon with DI water for a day and then drying out water at 80 °C in vacuum overnight. It was noted that, whereas the KB-DEN-RuO_2 mixture became homogenous instantaneously, the control KB took more than 15 min to disperse in water. This further shows the ability of amphiphilic dendrimers in increasing the dispersability of hydrophobic KB carbon in water by adsorbing on their surface. Once the electrode materials were dry, they were used to prepare the air electrodes. For KB-DEN-RuO_2, no binder was used. Using a homogenizer, KB-DEN-RuO_2 was mixed with toluene to make slurry that then was cast on a hydrophobic carbon paper (Torey Teflon coated carbon paper) using a brush. The coated carbon paper was then allowed to air-dry to remove toluene, and 1.4-cm-diameter electrodes with a loading of ~1 mg/cm^2 were punched. The electrodes were dried at 80 °C in vacuum overnight and transferred into the glove box for battery assembly. As controls, KB-PE electrodes were prepared similarly except that 20 wt% PE binder was added at the homogenizing step. The DEN-RuO_2 electrodes were prepared by first removing water from the DEN-RuO_2 solutions by drying in vacuum at 80 °C and then dispersing them in anhydrous methanol. The DEN-RuO_2 solution in methanol was then drop-casted on hydrophobic carbon paper and dried in vacuum at 80 °C overnight for battery fabrication. The surface areas and pore volumes of the electrode materials were determined by the BET and BJH methods, respectively, using N_2 adsorption/desorption collected with a Quantachrome Autosorb-6B gas sorption system on degassed samples. The electrolyte solution of 1.0 M LiTf in tetraglyme was prepared in an Ar-filled glove box (MBraun) with O_2 and H_2O <5 ppm. Perforated coin-cell type Li-O_2 batteries (type CR2032, MTI Corp.) were assembled in the Ar-filled glove box. A Li disk (1.5 cm in diameter and 1 mm thick) on a stainless-steel spacer was used as the anode. The anode was separated from the air cathode by a Celgard poly(propylene) membrane and a glass microfiber filter paper (Whatman GF/B), both 1.9 cm in diameter. The electrolyte of 240 µL was added to the cell and the cell was sealed using a hydraulic crimping machine. Because wetting G4-OH PAMAM dendrimers in polar aprotic solvents typically takes 24 hours, the assembled cells were placed in the glove box for one day to allow complete electrolyte wetting of the cathode materials. The batteries were tested at room temperature in Teflon containers filled with dry O_2 at 1 atm on an Arbin BT-2000 battery tester at a current density of 0.1 mA/cm^2. The batteries with only DEN-RuO_2 as cathode materials were tested at a current density of 0.01 mA/cm^2. The cells were cycled with a discharging voltage limit of 2 V and a charging that was stopped at a capacity the same as the discharge capacity in the previous step. The discharged batteries were disassembled in the glove box. The discharged electrodes were removed, soaked, washed with DME three times, dried in vacuum overnight, and then analyzed by various methods.

Characterization of Charged/Discharged Electrodes: SEM images were obtained with a FEI Quanta instrument at 5 kV. Samples were transferred in airtight containers from the glove box to the instrument. XRD analyses were done using a Rigaku D/Max Rapid II goniometer coupled to a MicroMax 007HF generator equipped with a rotating Cr anode (λ = 2.2910 Å). Samples were prepared by scraping the powder from the electrode and placing a small amount in a 300 µm glass capillary tube that then was wax-sealed before transferring from the glove box. The X-ray beam was focused through a 300 µm diameter collimator onto the sample and diffracted intensities integrated from a two-dimensional (2D) image plate detector. CV measurements were conducted on a CHI 660D potentiostat/galvanostat. Electrodeposition of the DEN-RuO_2 on the GC electrodes was done using a previously reported method (Figure S7).[44] The GC electrodes were polished with 0.3 µm gamma alumina powder followed by sonication in water for 10 min. The electrodes then were rinsed with water and ethanol and dried under flowing N_2 gas. All electrochemical deposition experiments were performed in a three-necked glass cell using a standard three-electrode cell with a Pt-gauze counter electrode and 0.01 M $AgClO_4$/0.1 M tributylammonium bis(trifluoromethanesulfonyl)imide (TBA-TFSI) in triglyme reference electrode (3.47 V vs Li). A freshly polished GC electrode was placed in an aqueous 20 µM DEN-RuO_2 solution containing 0.1 M $LiClO_4$, and then the potential of the electrode was scanned three times between 0 and 1.0 V (vs 0.01 M $AgClO_4$/0.1 M TBA-TFSI in triglyme). This resulted in robust immobilization of the DEN-RuO_2 on the GC. The GC electrode immobilized with DEN-RuO_2 then was rinsed with water and dried in vacuum at 50 °C overnight. The electrochemical cell for the CV measurements was assembled and sealed in the Ar-filled glove box. A 1 M LiTf-4G solution was used as the electrolyte, and Li foil was used as the counter and reference electrode. The GC electrode with DEN-RuO_2 was used as the working electrode. After testing in Ar, the electrolyte was saturated with dry O_2. The O_2 atmosphere was maintained inside the cell throughout the measurements. For the Raman analysis of the DEN-RuO_2 electrodes, the setup has been described elsewhere.[45] Surface-enhanced Raman spectroscopy (SERS) measurements were conducted using an inverted optical microscopy setup (Axiovert 200, Zeiss). The incident 514 nm continuous wave laser light (Innova 300, Coherent) was attenuated using a variable neutral density filter wheel (40–100 µW/µm^2), reflected off a dichroic beamsplitter, and focused onto the sample surface using a standard air objective. The backscattered radiation is collected through the same objective, transmitted though the dichroic beamsplitter, and filtered through a long pass filter. The resulting light is detected by a liquid nitrogen cooled charge coupled device coupled (CCD) to a spectrometer (Holespec f/1.8i, Kaiser Optical System). The effective instrument resolution in the micro-Raman experiments is ~8 cm^{-1}.

Supporting Information

Supporting Information is available from the Wiley Online Library or from the author.

Acknowledgements

This work was supported by U.S. Department of Energy (DOE) Laboratory Directed Research and Development funding at Pacific Northwest National Laboratory (PNNL). A portion of the research was performed using Environmental Molecular Sciences Laboratory (EMSL), a national scientific user facility sponsored by the DOE Office of Biological and Environmental Research and located at PNNL. PNNL is operated for the DOE by Battelle. PB is grateful for support from a Linus Pauling Distinguished Postdoctoral Fellowship at PNNL. The authors wish to thank Drs. Yuyan Shao, Teresa Lemmon and Patrick El Khoury at PNNL for their help and useful discussions on the CV, ICP-MS, and Raman measurements, respectively.

Received: August 8, 2014
Revised: August 23, 2014
Published online: September 17, 2014

[1] Y.-C. Lu, B. M. Gallant, D. G. Kwabi, J. R. Harding, R. R. Mitchell, M. S. Whittingham, Y. Shao-Horn, *Energy Environ. Sci.* **2013**, *6*, 750.
[2] Y. Shao, S. Park, J. Xiao, J.-G. Zhang, Y. Wang, J. Liu, *ACS Catal.* **2012**, *2*, 844.
[3] B. D. McCloskey, A. Speidel, R. Scheffler, D. C. Miller, V. Viswanathan, J. S. Hummelshøj, J. K. Nørskov, A. C. Luntz, *J. Phys. Chem. Lett.* **2012**, *3*, 997.

[4] M. M. O. Thotiyl, S. A. Freunberger, Z. Peng, P. G. Bruce, *J. Am. Chem. Soc.* **2013**, *135*, 494.
[5] B. D. McCloskey, R. Scheffler, A. Speidel, D. S. Bethune, R. M. Shelby, A. C. Luntz, *J. Am. Chem. Soc.* **2011**, *133*, 18038.
[6] B. Sun, P. Munroe, G. Wang, *Sci. Rep.* **2013**, *3*, 2247.
[7] H. -G. Jung, Y. S. Jeong, J. -B. Park, Y. -K. Sun, B. Scrosati, Y. J. Lee, *ACS Nano* **2013**, *7*, 3532.
[8] E. Yilmaz, C. Yogi, K. Yamanaka, T. Ohta, H. R. Byon, *Nano Lett.* **2013**, *13*, 4679.
[9] J. R. Harding, Y.-C. Lu, Y. Tsukada, Y. Shao-Horn, *Phys. Chem. Chem. Phys.* **2012**, *14*, 10540.
[10] R. M. Crooks, M. Zhao, L. Sun, V. Chechik, L. K. Yeung, *Accounts Chem. Res.* **2001**, *34*, 181.
[11] V. S. Myers, M. G. Weir, E. V. Carino, D. F. Yancey, S. Pande, R. M. Crooks, *Chem. Sci.* **2011**, *2*, 1632.
[12] R. W. Scott, O. M. Wilson, R. M. Crooks, *J. Phys. Chem. B* **2005**, *109*, 692.
[13] P. Bhattacharya, N. K. Geitner, S. Sarupria, P. C. Ke, *Phys. Chem. Chem. Phys.* **2013**, *15*, 4477.
[14] M. Zhao, R. M. Crooks, *Angew. Chem. Int. Edit.* **1999**, *38*, 364; *Angew. Chem.* **1999**, *111*, 375.
[15] M. Zhao, R. M. Crooks, *Adv. Mater.* **1999**, *11*, 217.
[16] L. K. Yeung, R. M. Crooks, *Nano Lett.* **2001**, *1*, 14.
[17] V. Chechik, M. Zhao, R. M. Crooks, *J. Am. Chem. Soc.* **1999**, *121*, 4910.
[18] L. N. Lewis, *Chem. Rev.* **1993**, *93*, 2693.
[19] D. E. Bergbreiter, Y.-S. Liu, *Tetrahedron Lett.* **1997**, *38*, 7843.
[20] S.-K. Oh, Y. Niu, R. M. Crooks, *Langmuir* **2005**, *21*, 10209.
[21] Y. Li, M. A. El-Sayed, *J. Phys. Chem. B* **2001**, *105*, 8938.
[22] P. B. Amama, M. R. Maschmann, T. S. Fisher, T . D. Sands, *J. Phys. Chem. B* **2006**, *110*, 10636.
[23] P. Tartaj, M. del Puerto Morales, S. Veintemillas-Verdaguer, T. González-Carreno, C. J. Serna, *J. Phys. D. Appl. Phys.* **2003**, *36*, R182.
[24] G. Lafaye, A. Siani, P. Marécot, M. D. Amiridis, C. T. Williams, *J. Phys. Chem. B* **2006**, *110*, 7725.
[25] G. Lafaye, C. T. Williams, M. D. Amiridis, *Catalysis Lett.* **2004**, *96*, 43.
[26] D. Liu, Y. M. López-De Jesús, J. R. Monnier, C. T. Williams, *J. Catal.* **2010**, *269*, 376.
[27] N. C. Antonels, R. Meijboom, *Langmuir* **2013**, *29*, 13433.
[28] C. Ingemar Odenbrand, S. L. T. Andersson, *J. Chem. Technol. Biot.* **1982**, *32*, 365.
[29] M. Guglielmi, P. Colombo, V. Rigato, G. Battaglin, A. Boscolo-Boscoletto, A. DeBattisti, *J. Electrochem. Soc.* **1992**, *139*, 1655.
[30] L. Garvie, P. R. Buseck, *J. Phys. Chem. Solids* **1999**, *60*, 1943.
[31] C. Bianchi, V. Ragaini, M. Cattania, *Mater. Chem. Phys.* **1991**, *29*, 297.
[32] D. Briggs, M. P. Seah, *Practical Surface Analysis by Auger and X-Ray Photoelectron Spectroscopy*, Wiley, Chichester **1983**.
[33] P. Froment, M. Genet, M. Devillers, *J. Electron. Spectrosc. Relat. Phenom.* **1999**, *104*, 119.
[34] K.-H. Chang, C.-C. Hu, *J. Electrochem. Soc.* **2004**, *151*, A958.
[35] O. Ozturk, T. Black, K. Perrine, K. Pizzolato, C. Williams, F. Parsons, J. Ratliff, J. Gao, C. Murphy, H. Xie, *Langmuir* **2005**, *21*, 3998.
[36] J. Walker, R. Bruce King, R. Tannenbaum, *J. Solid State Chem.* **2007**, *180*, 2290.
[37] E. A. Seddon, K. R. Seddon, R. J. Clark, *The Chemistry of Ruthenium*, Elsevier, Amsterdam **1984**.
[38] K. C. Taylor, *J. Catal.* **1975**, *38*, 299.
[39] B. Herd, J. C. Goritzka, H. Over, *J. Phys. Chem. C* **2013**, *117*, 1519.
[40] N. Garcia-Araez, P. Novák, *J. Solid State Electr.* **2013**, *17*, 1793.
[41] E. Nasybulin, W. Xu, M. H. Engelhard, Z. Nie, X. S. Li, J.-G. Zhang, *J. Power Sources* **2013**, *243*, 899.
[42] L. Peyser-Capadona, J. Zheng, J. I. Gonza'lez, T.-H. Lee, S. A. Patel, R. M. Dickson, *Phys. Rev. Lett.* **2005**, *94*, 058301.
[43] B. M. Gallant, R. R. Mitchell, D. G. Kwabi, J. Zhou, L. Zuin, C. V. Thompson, Y. Shao-Horn, *J. Phys. Chem. C* **2012**, *116*, 20800.
[44] H. Ye, R. M. Crooks, *J. Am. Chem. Soc.* **2005**, *127*, 4930.
[45] P. Z. El-Khoury, D. Hu, V. A. Apkarian, W. P. Hess, *Nano Lett.* **2013**, *13*, 1858.